

JGR Atmospheres

,

RESEARCH ARTICLE

10.1029/2023JD039926

Key Points:

- Weather radar estimates of biomass burning debris injection heights are evaluated against aerosol heights from airborne lidar
- Radar maximum injection heights tend to be overpredicted while mean, median, 75th and 90th percentiles perform better
- The maximum injection height can be predicted generally well by the 75th to 90th percentiles of the radar estimates

Correspondence to:

M. Krishna and P. E. Saide, mansakrishna23@ucla.edu; saide@atmos.ucla.edu

Citation

Krishna, M., Saide, P. E., Ye, X., Turney, F. A., Hair, J. W., Fenn, M., & Shingler, T. (2024). Evaluation of wildfire plume injection heights estimated from operational weather radar observations using airborne Lidar retrievals. *Journal of Geophysical Research: Atmospheres*, 129, e2023JD039926. https://doi.org/10.1029/2023JD039926

Received 1 SEP 2023 Accepted 8 APR 2024

Author Contributions:

Concentualization: M. Krishna P. E. Saide Data curation: M. Krishna, J. W. Hair, M. Fenn, T. Shingler Formal analysis: M. Krishna, P. E. Saide Funding acquisition: P. E. Saide Investigation: M. Krishna, P. E. Saide, X. Ye. F. A. Turney Methodology: M. Krishna, P. E. Saide, X. Ye, F. A. Turney Project administration: P. E. Saide Resources: P. E. Saide, X. Ye, F. A. Turney, J. W. Hair, M. Fenn, T. Shingler Software: M. Krishna, P. E. Saide, X. Ye, F. A. Turney Supervision: P. E. Saide, X. Ye,

© 2024 The Authors.

F. A. Turney

This is an open access article under the terms of the Creative Commons Attribution-NonCommercial License, which permits use, distribution and reproduction in any medium, provided the original work is properly cited and is not used for commercial purposes.

Evaluation of Wildfire Plume Injection Heights Estimated from Operational Weather Radar Observations Using Airborne Lidar Retrievals

M. Krishna^{1,2} , P. E. Saide^{1,3} , X. Ye^{1,4}, F. A. Turney¹ , J. W. Hair⁵ , M. Fenn⁵ , and T. Shingler⁵

¹Department of Atmospheric and Oceanic Sciences, University of California, Los Angeles, CA, USA, ²Department of Earth Sciences, Dartmouth College, Hanover, NH, USA, ³Institute of the Environment and Sustainability, University of California, Los Angeles, CA, USA, ⁴Institute of Urban Environment, Chinese Academy of Sciences, Xiamen, China, ⁵NASA Langley Research Center, Hampton, VA, USA

Abstract The vertical distribution of wildfire smoke aerosols is important in determining its environmental impacts but existing observations of smoke heights generally do not possess the temporal resolution required to fully resolve the diurnal behavior of wildfire smoke injection. We use Weather Surveillance Radar-1988 Doppler (WSR-88D) dual polarization data to estimate injection heights of Biomass Burning Debris (BBD) generated by fires. We detect BBD as a surrogate for smoke aerosols, which are often collocated with BBD near the fire but are not within the size range detectable by these radars. Injection heights of BBD are derived for 2-10 August 2019, using WSR-88D reflectivity ($Z \ge 10$ dBZ) and dual polarization correlation coefficients (0.2 < C.C < 0.9) to study the Williams Flats fire. Results show the expected diurnal cycles with maximum injection heights present during the late afternoon period when the fire's intensity and convective mixing are maximized. WSR-88D and airborne lidar injection height comparisons reveal that this method is sensitive to outliers and generally overpredicts maximum heights by 40%, though mean and median heights are better captured (<20% mean error). WSR-88D heights between the 75th and 90th percentile seem to accurately represent the maximum heights, with the exception of heights estimated during the occurrence of a pyrocumulonimbus. Location specific mapping of WSR-88D and lidar injection heights reveal that they diverge further away from the fire as expected due to BBD settling. Most importantly, WSR-88D-derived injection height estimates provide near continuous smoke height information, allowing for the study of diurnal variability of smoke injections.

Plain Language Summary Wildfire smoke aerosols injected into the atmosphere pose a serious threat to human health and the environment. Once in the atmosphere, these aerosols can be transported downwind, affecting air quality regionally. Aerosols advected downwind travel distances that are strongly correlated with the maximum heights that aerosols can reach near their source, making it important to observe these 'injection heights'. However, existing observations of injection heights are limited temporally, making it difficult to study their diurnal and day-to-day variability. Here, we use weather radar data to estimate the injection heights of Biomass Burning Debris (BBD), which is assumed to be collocated with aerosols that are too small to be detected by these radars. Injection heights are estimated for the Williams Flats Fire event in Washington for 2–10 August 2019. Results show that daily maximum injection heights occur in the late afternoon, when the wildfire's intensity is strongest. Further, weather radar-derived heights are compared to airborne lidar-derived heights for the same fire, revealing that the maximums are overpredicted but intermediate values like the mean are well represented. Weather radar-derived injection height estimates allow for near continuous smoke heights, making them relevant for future studies.

1. Introduction

The issue of air quality is a pressing concern due to the rapidly developing global economy and increased industrialization and urbanization (Manisalidis et al., 2020). Not only is the deterioration of air quality significant due to its environmental and ecological impacts, but also due to the health risk it poses for humans (Gakidou et al., 2017). Wildfires contribute to this burden on human health by emitting smoke aerosols into the atmosphere (Balmes, 2020), which is a rising concern as the number of catastrophic wildfires worldwide are increasing with climate change (Deb et al., 2020; Higuera & Abatzoglou, 2021). Furthermore, wildfire smoke

KRISHNA ET AL. 1 of 13

Validation: P. E. Saide, X. Ye, F. A. Turney Visualization: M. Krishna, P. E. Saide Writing – original draft: M. Krishna Writing – review & editing: M. Krishna, P. E. Saide, X. Ye, F. A. Turney, J. W. Hair, M. Fenn, T. Shingler aerosols injected into the atmosphere above the boundary layer can undergo long range transport and affect surface air quality in downwind regions (Buchholz et al., 2022; Hung et al., 2020; Schum et al., 2018). The injection heights of these aerosols in the atmosphere are closely related to the residence time of aerosols in the atmosphere and the distance they are transported (Schum et al., 2018), implying that greater injection heights could lead to more widespread impacts on air quality, making it important to better observe the vertical distribution of these smoke aerosols.

According to prior studies, smoke injection heights have been estimated in multiple ways. Multiple space-based estimation techniques exist, including the vertical profiles of aerosol and cloud backscatter provided by the Cloud-Aerosol Lidar with Orthogonal Polarization (CALIOP) instrument (Amiridis et al., 2010; Winker et al., 2004) and using the smoke height products retrieved from various passive remote sensing instruments such as the Multi-angle Imaging SpectroRadiometer (MISR) (M. Val Martin et al., 2010; Maria Val Martin et al., 2018), the Tropospheric Monitoring Instrument (TROPOMI) (Chen et al., 2021; Michailidis et al., 2022; Veefkind et al., 2012), the Moderate Resolution Imaging Spectroradiometer (MODIS), and the Visible Infrared Imaging Radiometer Suite (VIIRS) (Hsu et al., 2019; Lee et al., 2015; Loría-Salazar et al., 2021; Sayer et al., 2019). However, these retrievals are limited by the fact that the sun-synchronous orbits of all these satellites only allow for one or two overpasses in a given day (Maria Val Martin et al., 2018). Though stereo imaging from a pair of geostationary (GEO) satellites with overlapping coverage is able to overcome the aforementioned limitation, this method has not been extensively validated and is only available during the daytime (Carr et al., 2020; Hasler, 1981). Thus, there is a need to develop and evaluate smoke injection height estimates that cover full diurnal cycles and have the potential to provide real-time measurements.

Here, we explore the use of the Weather Surveillance Radar-1988 Doppler (WSR-88D), an under-utilized tool for studying wildfires (McCarthy et al., 2019). Since smoke aerosols are often collocated with lofted debris in the vicinity of the fire, the WSR-88D can be used to retrieve the injection heights of Biomass Burning Debris (BBD), also referred to as pyrometeors (McCarthy et al., 2019), produced from wildfires as a possible surrogate for the injection heights of smoke aerosol plumes (Jones & Christopher, 2009). The significance of this approach is that it possesses adequate spatial and temporal coverage and allows for the retrieval of a complete time series of plume injection heights and depicts day-to-day variability of the same (Jones & Christopher, 2009). While radar estimates of wildfire plume structure are being used to evaluate models (Shamsaei et al., 2023), they have not yet been thoroughly compared to more established observations of smoke plume height. Drawing inspiration from Jones and Christopher (2009), who have previously provided hourly injection heights over a 2-day period, we retrieved plume injection heights for the whole lifetime of a fire and performed an evaluation of these retrievals. In the following study, we describe the methods used to derive smoke injection heights from WSR-88D data, show results for the 2019 Williams Flats Fire, and evaluate them using airborne lidar data from the Fire Influence on Regional to Global Environments and Air Quality (FIREX-AQ) field campaign (Warneke et al., 2023). Conclusions and future directions are outlined in the sections to follow.

2. Data and Methods

2.1. Weather Surveillance Radar-1988 Doppler (WSR-88D)

The WSR-88D network spread through the United States currently consists of 160 S-Band (10 cm) precipitation radars operated by the National Oceanic and Atmospheric Administration National Weather Service (Crum & Alberty, 1993; Holleman et al., 2022). Radars in the WSR-88D network can operate in two modes (i.e., clear-air mode and precipitation mode) and characterize echoes through reflectivity, correlation coefficient, mean radial velocity, spectrum width, etc (Crum & Alberty, 1993; Doviak et al., 2000). In either clear-air and precipitation mode, the WSR-88D is operated in one of many Volume Coverage Patterns (VCPs), which consists of the radar antenna making a series of 360° scans of the surrounding atmosphere for pre-determined, increasing elevation angles (Crum & Alberty, 1993; Kingfield & French, 2022; NOAA National Weather Service et al., 2023).

The localized instability and increased buoyancy produced by the heat of a wildfire may result in the lofting of significant amounts of debris, ash, and other particulate matter several kilometers into the atmosphere (Kingsmill et al., 2023; Rodriguez et al., 2020; Thurston et al., 2017). It is important to note that smoke particles (diameter $D < 20\mu$ m) are generally too fine to be detected by the WSR-88D, but BBD (diameter D > 1 mm) are more easily detected by these weather surveillance radars (Banta et al., 1992; McCarthy et al., 2019).

KRISHNA ET AL. 2 of 13

2.2. Data Collected: Reflectivity and Correlation Coefficient Characteristics

To estimate the plume injection heights of BBD for the 2019 Williams Flats Fire event in northeast Washington, ~216 hr (from 00:04:38 on 2 August 2019 to 00:04:47 on 11 August 2019) of Level II WSR-88D data were obtained from a single weather surveillance radar (KOTX) (DOC/NOAA/NWS/ROC, 1991), which is approximately 80 km from the fire. During this period, the WSR-88D operated in two modes: VCP-35 (clear-air mode) and VCP-215 (precipitation mode). When operated in VCP-35, WSR-88D data are collected at 9 elevation angles (0.5°, 0.9°, 1.3°, 1.8°, 2.4°, 3.1°, 4.0°, 5.1°, and 6.4°) approximately every 7 min, whereas in VCP-215, data are collected for 15 elevation angles (VCP-35 angles, 8.0°, 10.0°, 12.0°, 14.0°, 16.7°, and 19.5°) approximately every 6 min (NOAA National Weather Service et al., 2023). The WSR-88D's reflectivity range resolution, azimuth resolution, and beamwidth are 1 km, 1°, and ~1° respectively (National Research Council, 2002).

The WSR-88D is designed to detect atmospheric scatterers or precipitation-sized hydrometeors (diameter $D > 100\mu$ m) from backscattered electromagnetic energy in the microwave spectrum and the returned energy is used to determine the reflectivity (measured in dBZ) (Donald Burgess & Peter S. Ray, 1986). The WSR-88D is also designed to detect how similarly the horizontally and vertically polarized returns (of energy) are behaving; this similarity is quantified using the correlation coefficient (Doviak et al., 2000). Atmospheric scatterers that are highly variable in size and shape (such as debris or birds) will likely have less similarly behaving horizontal and vertical returns, leading to lower correlation coefficient values (Melnikov et al., 2008; Zrnic et al., 2020); scatterers that are more uniform in size and shape (such as rain droplets or snow) will have more similarly behaving horizontal and vertical returns, leading to higher correlation coefficient values (Liu & Chandrasekar, 2000).

Radar reflectivity and correlation coefficient data from the aforementioned WSR-88D were passed through the injection height estimation algorithm (details provided in Section 2.3) and hence used to estimate the injection heights of smoke aerosols.

2.3. Injection Height Estimation Algorithm

The following injection height estimation algorithm uses Py-ART, a Python module developed for parsing weather surveillance radar data (Helmus & Collis, 2016). The WSR-88D data (i.e., the reflectivity and correlation coefficient data) were re-gridded from the native radar polar coordinates into cartesian coordinates (latitude, longitude, and altitude) using the "grid_from_radars" function within Py-ART and then passed through the injection height estimation algorithm developed for this study. The algorithm works by analyzing a pre-determined, three-dimensional grid around a given fire. Here, we studied the 2019 Williams Flats Fire (located at 47.98°N latitude, -118.624°E longitude) (Peterson et al., 2022; Ye et al., 2021, 2022), with the pre-determined grid defined to extend from 47.85°N to 48.05°N latitude and -118.70°E to -118.20°E longitude. The horizontal grid spacing is set to be ~1,000 m, matching the radar range resolution. The vertical spacing of the radar beams can be estimated as the difference between the height of the center of the beams at consecutive angles, which at 80 km (distance between radar and fire ignition) from the radar is 500–700m for the first four angles (0–2.5 km altitude) and increases from there (e.g., ~1 km resolution at ~4 km altitude, ~2 km resolution at 9–11 km altitude). The vertical spacing matches the beamwidth at the lowest scans and thus this vertical spacing can be used to estimate the radar vertical resolution at these levels. Thus, the vertical resolution of the pre-determined, three-dimensional grid was set 500 m to retain most of the radar vertical information at lower levels. At each timestamp, the algorithm was initially designed to search for vertical regions of contiguous reflectivity exceeding or equal to a defined minimum reflectivity threshold and return the maximum injection height if the reflectivity value fell below the minimum threshold (Figure 1a). For each (x,y) position within the pre-determined grid, the algorithm can search up to a height of 14,727 m in 500 m increments (Note that the height of the radar is 727 m above sea

Previous studies utilized polarimetric data to identify smoke plumes, observing reflectivity values on the range of 10–25 dBZ (Lang et al., 2014; Zrnic et al., 2020). Therefore, based on the existing literature, reflectivity threshold values for lofted debris were tested in a range of 5–20 dBZ (Figure 2a). We considered 10 dBZ to be an appropriate minimum threshold as the 5 dBZ threshold generated heights that likely did not correspond to the smoke top since fire activity was very low between 14 and 19 UTC and thresholds of 15 dBZ and 20 dBZ produced significantly lower heights for the more active fire period after 20 UTC (Ye et al., 2021). The 10 dBZ threshold is also consistent with assumptions made in Jones and Christopher (2009).

KRISHNA ET AL. 3 of 13

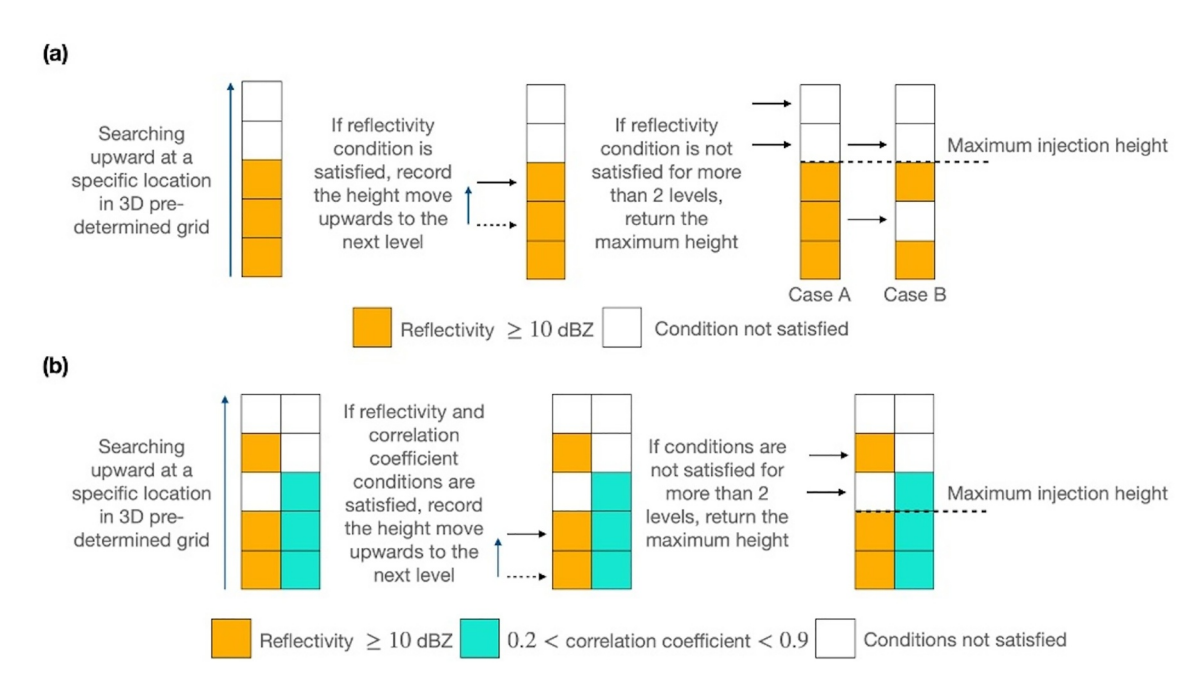


Figure 1. Upper panel (a): Diagrammatic representation of initial version of the injection height estimation algorithm (left) The algorithm searches upwards, through each grid square within the pre-determined grid, for regions of contiguous reflectivity (middle) the algorithm searches upwards iteratively, checking if the current region satisfies the reflectivity threshold (right) the algorithm returns the last height for which the reflectivity threshold was satisfied if 2 'bad' reflectivity values are retrieved. The algorithm allows a buffer of 2 'bad' reflectivity values before retrieving the maximum height; case A depicts a contiguous reflectivity situation whereas case B depicts a (likely rare) discontiguous reflectivity situation. Lower panel (b): Similar to (a) but for the modified version of the injection height estimation algorithm (left) The algorithm iteratively searches upwards through each grid square (middle) moving upwards to the next grid square if the reflectivity and correlation coefficient conditions are satisfied (right) The algorithm allows a buffer of 2 'bad' reflectivity or correlation coefficient values before retrieving the maximum injection height.

The Williams Flats Fire, first reported at 10:23 UTC on 2 August 2019, was ignited by lightning strikes associated with the thunderstorm ~80 km northwest of the WSR-88D (KOTX) (Ye et al., 2021). Therefore, the initial algorithm (Figure 1a) ran the risk of retrieving heights of atmospheric scatterers whose reflectivity exceeded the minimum threshold of 10 dBZ and were likely not BBD, but instead were more likely the hydrometeors present in the thunderstorm that initiated the fire. Attempts were made to discriminate between BBD and hydrometeors by setting an upper bound on the reflectivity values (Figure 2b), but this did not help in discriminating between BBD and the hydrometeors from the thunderstorm. Hence, other approaches were tested. A correlation coefficient constraint was embedded within the algorithm to curb the possible overestimation of injection heights; heights were only retrieved if both the reflectivity and correlation coefficient conditions were satisfied to improve the injection height retrievals when rain or snow was present (Figure 1b). Based on existing literature, correlation coefficient values inside smoke plumes tend to be below 0.8 (Melnikov et al., 2008; Zrnic et al., 2020) and rain or drizzle tends to have values above 0.9 (Liu & Chandrasekar, 2000), and thus a range of 0.2-0.9 was assumed for detecting BBD. Results from the version of the algorithm including the correlation coefficient mask are discussed in Sections 3 and 4. This modification proved to be effective in discriminating between debris and hydrometeors as the injection heights retrieved for 2 August 2019 with the modified algorithm successfully eliminated the convective system (Figure 2c).

2.4. Data Sets Used as Reference for Evaluation

The Differential Absorption Lidar (DIAL)—High Spectral Resolution Lidar (HSRL) (Hair et al., 2018) from the DC-8 aircraft during the FIREX-AQ field campaign was used as a reference. The DC-8 sampled the Williams Flats Fire plume on 3, 6, and 7 August 2019 (PST), capturing multiple phases of the fire. Images of 11 transects overpassing the Williams Flats Fire on these days can be found in Ye et al. (2021). The DIAL-HSRL system is capable of providing measurements of aerosol depolarization (355, 532, 1,064 nm), aerosol/cloud extinction (532 nm), and backscatter coefficients (355, 532, 1,064 nm) above and below flight height at a temporal resolution of 10 s. Maximum smoke injection heights were derived based on the vertical gradients of 532 nm backscatter

KRISHNA ET AL. 4 of 13

21698996, 2024, 9, Downloaded from https://agupubs.onlinelibrary.wiley.com/doi/10.1029/2023JD039926 by University Of California, Los, Wiley Online Library on [03/07/2024]. See the Terms and Conditions (https://onlinelibrary.wiley.com/terms/

and-conditions) on Wiley Online Library for rules

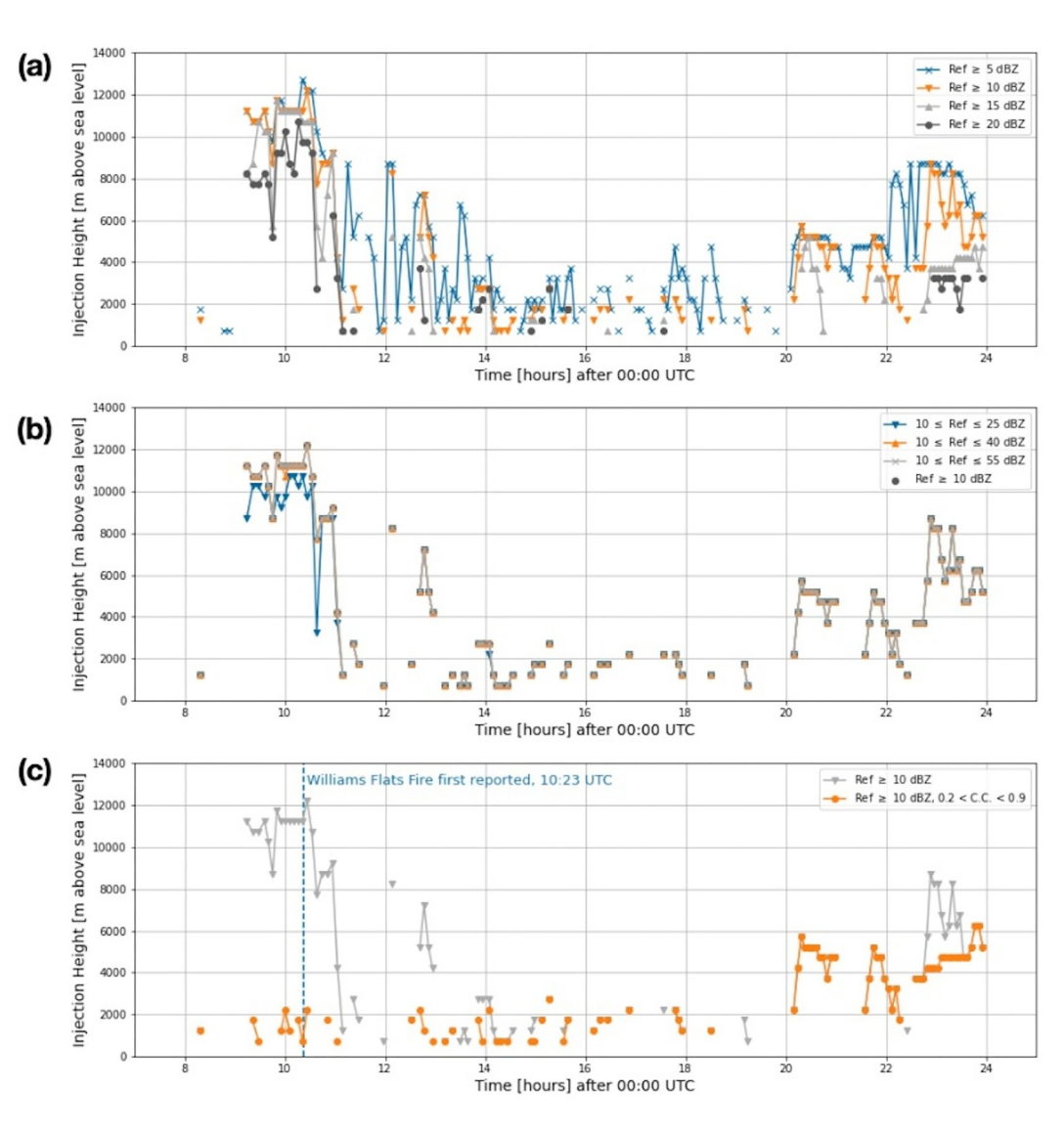


Figure 2. Injection heights estimated on 2 August 2019 (UTC). (a) Heights estimated using different lower bounds of reflectivity values: 5, 10, 15, and 20 dBZ. The appropriate minimum threshold chosen was 10 dBZ. (b) Heights estimated using minimum reflectivity threshold of 10 dBZ and different upper reflectivity thresholds: 25, 40, and 55 dBZ. (c) Heights estimated using the initial (gray) and modified (orange) algorithms. The extremely high injection heights (upwards of 10 km above sea level) occur around the time the Williams Flats Fire began (dotted, blue vertical line), leading to the conclusion that the initial algorithm was likely detecting hydrometeors from the early morning thunderstorm in the Colville Reservation, WA. The correlation coefficient constraint within the modified algorithm successfully reduces the heights retrieved.

coefficients, and are used in this study (Ye et al., 2021). It should be noted that while the lidar footprint is narrow, the measuring strategy implemented in FIREX-AQ consisted on doing an overpass at altitude across the axis of the plume, followed by several plume crossings at increasing distances downwind of the fire (Warneke et al., 2023). Since DIAL-HSRL detects aerosols that do not settle rapidly (as is likely the case with BBD), the measurement strategy allows us to say with confidence that the retrieved heights are an accurate representation of the whole plume.

Geostationary satellite imagery produced specifically for FIREX-AQ by the Florida State University team was used to provide context regarding smoke and aircraft location (Warneke et al., 2023). Airborne lidar and satellite imagery are available in the FIREX-AQ data repository (NASA/LARC/SD/ASDC, 2020).

KRISHNA ET AL. 5 of 13

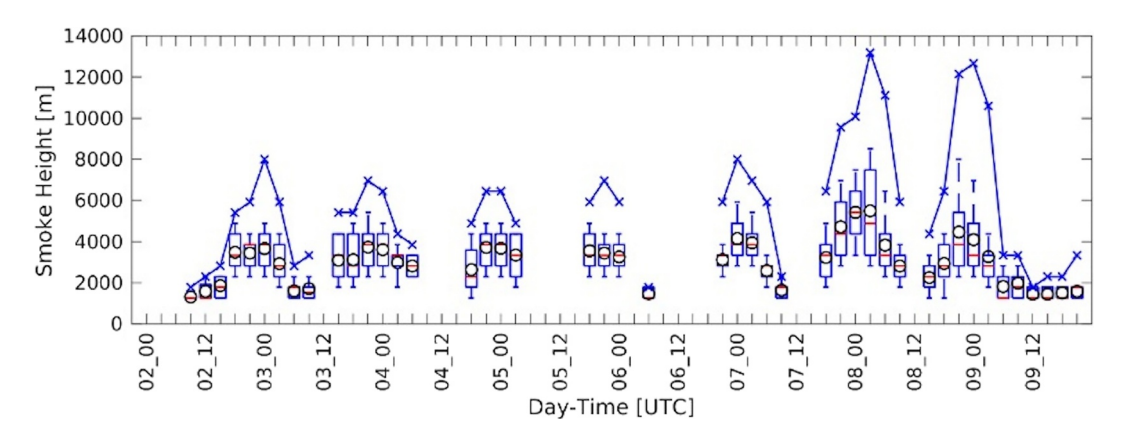


Figure 3. Box and whisker plots depicting an extended time series of radar-derived smoke injection heights (2–10 August 2019) aggregated over 3-hr intervals. Central, solid lines (red) indicate the median, circles (black) indicate the mean, boxes indicate the lower and upper quartiles, whiskers indicate the upper and lower deciles, and the crosses connected with solid lines indicate the maximums. The time series captures the diurnal cycle of fires, displaying that the daily maximum injection heights are present during the late afternoon period. Visible gaps in the time series occur when the reflectivity and correlation coefficient conditions are not satisfied or when there were less than 10 samples in each time interval.

3. Results

3.1. Timeseries of Injection Heights

Using the injection height estimation algorithm including both reflectivity and correlation coefficient thresholds (detailed in Section 2.3), an extended time series of the plume injection heights was retrieved for the 2019 Williams Flats Fire event (Figure 3). It should be noted that the time series captures the typical diurnal cycle of fires, with daily maximums occurring during the latter half of the day when the fire's intensity and convective mixing is maximized (Jones & Christopher, 2009; Zrnic et al., 2020). We also note that despite regular retrievals of WSR-88D data, there are visible gaps in the extended time series. This is likely due to the weak reflectivity observed during the morning period, suggesting that the buoyancy flux of the fire was not strong enough to lift sufficient BBD to meet the reflectivity threshold or the correlation coefficient constraint (Rodriguez et al., 2020; Tory et al., 2018). The time series also shows large differences between intermediate heights (i.e., heights within the 25–75th percentile range) and the maximum heights during the most intense periods of the diurnal cycles, sometimes reaching >6 km differences, which needs to be further assessed with reference observations.

3.2. Comparison to Injection Heights Retrieved From Airborne Lidar Data

To evaluate the algorithm's accuracy in retrieving injection heights of BBD, these were compared to the injection heights derived from airborne lidar data from the 2019 FIREX-AQ campaign. The flight path of the aircraft (with the airborne lidar) sampled the whole extent of the plume, going beyond the pre-determined grid used to retrieve the WSR-88D-derived injection heights (the red box (es) in Figures 4a–4c). Hence, the lidar-derived injection heights outside the pre-determined grid were removed for this comparison as BBD is expected to settle quickly and is therefore unlikely to match the smoke heights further away from the fire. Figure 5 shows distributions of injection heights for 3, 6, and 7 August 2019 (PST), the days when the aircraft was sampling this fire.

From Figure 5, it can be concluded that the distribution of maximum injection heights derived from WSR-88D data is significantly wider than the distribution of injection heights derived from the airborne lidar data. The maximum injection heights retrieved from the WSR-88D are overpredicted by ~2000 m, a 40% difference on average (Table 1). However, the mean, median, 75th and 90th percentiles seem to agree better with the injection heights derived from airborne lidar data (350–820 m mean error), though a general overprediction of heights persists (under the assumption that the airborne lidar data are the reference). Figure 5 also shows that the WSR-88D data are capable of capturing the increase in top injection heights from the third and sixth of August to the seventh, thus capturing the day-to-day variability. As mentioned above, the time series of heights derived from WSR-88D data has gaps when the fire intensity is not strong enough, however shallow smoke aerosol injections into the boundary layer could still be occurring during these periods (as seen during 18–20 UTC on 6 August 2019). On the other hand, each time free-tropospheric injections were detected by the lidar, the WSR-88D shows

KRISHNA ET AL. 6 of 13



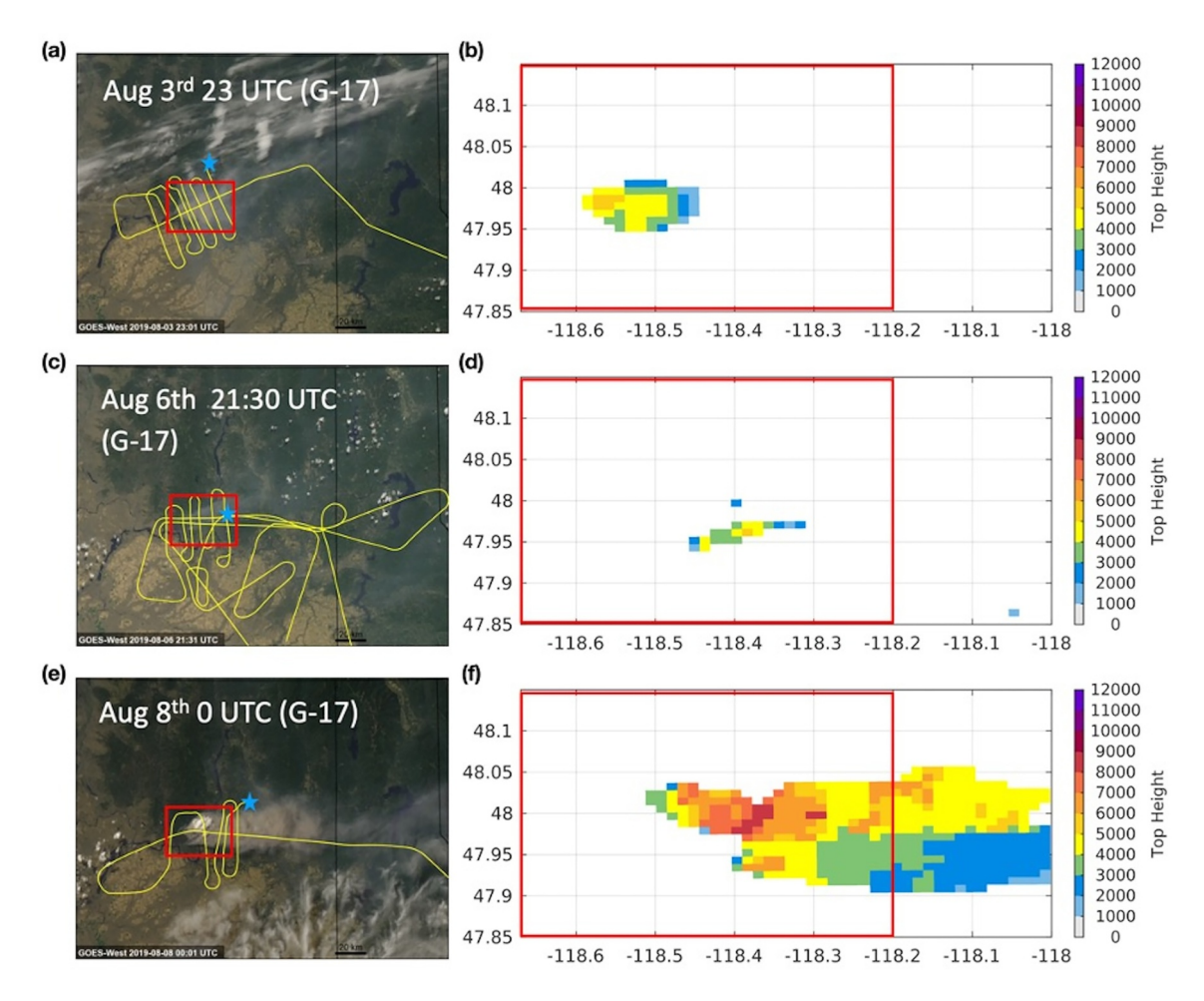


Figure 4. Left panels (a) (c) (e): FIREX-AQ flight paths (solid yellow lines) and pre-determined grid (red box) for flights on August 3, 6, and 7; Imagery from the GOES-17 satellite. The blue star represents the aircraft location at the indicated times. **Right panels** (b) (d) (f): Maps of maximum injection heights derived from the radar data for the corresponding times. The *x*-axis indicates longitude values in °E and the *y*-axis indicates latitude values in °N.

strong diurnal signals (Figures 5a and c). Thus, for applications using WSR-88D data to inject smoke into models, a fair assumption for injection when the radar signal is not available would be the top of the boundary layer.

The overprediction by the injection height estimation algorithm (using WSR-88D data) could be occurring for several reasons. One potential reason for the overprediction is that the algorithm is retrieving maximum injection heights for each timestamp within the pre-determined grid whereas the lidar-derived injection heights are retrieved according to the flight path. Therefore, there is a possibility that the WSR-88D and lidar-derived injection heights are different because they are being retrieved for different locations, implying that the lidar may be missing some short-lived increases in injection height. Hence, to make this comparison more robust, a location-specific injection height mapping was used. The injection heights were derived using the algorithm at the latitude-longitude position of the aircraft. Reflectivity cross-sections over the flight track with the associated injection heights were plotted accordingly (Figure 6).

After the location-specific mapping, we note that the maximum heights are much closer within the pre-determined grid around the fire (Table 2), with the mean error dropping to 1,160 m and near 0 bias. While bias is reduced, similar errors persist for other metrics (mean, median, and percentiles) (610–890 m). We also note that there are still some instances where the maximum injection height is largely overpredicted (e.g., 00 UTC on 4 August 2019, 01–02 UTC on 8 August 2019 in Figure 3). Previously mentioned in Section 2, the maximum injection heights for the whole domain should not substantially deviate from the lidar-derived injection heights due to the airborne lidar sampling strategy and the relatively low settling velocities of smoke aerosols. Thus, we hypothesize that the

KRISHNA ET AL. 7 of 13



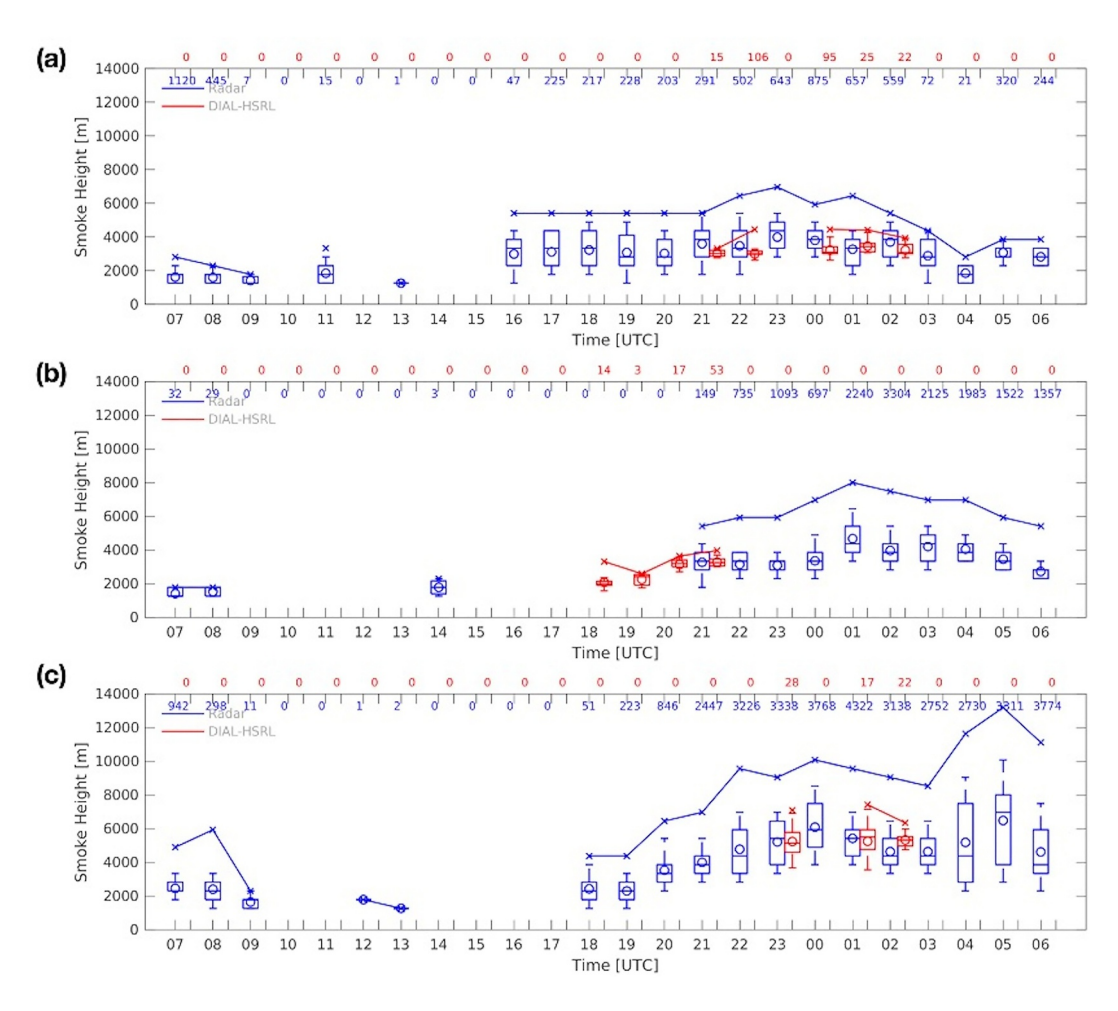


Figure 5. Box and whisker plots (similar to Figure 3) of the injection heights derived from both WSR-88D (blue) and airborne lidar (red) data for each hour (local time) on (a) 3 August 2019, (b) 6 August 2019, and (c) 7 August 2019. The number of data points for each hour is shown at the top of each panel, color-coded according to the corresponding box and whisker plot(s). For further details, see Table 1.

overprediction of maximum injection heights observed by the WSR-88D is due to outliers that are present throughout the time period of the fire. Reasons for this could include the coarse vertical spacing of the radar beams which is 1–2 km for these heights (Section 2.3), the possibility that the bottom of the radar beam grazes the smoke plumes which could produce reflectivities above the threshold due to the high detectability of the WSR-88D (Crum et al., 1998), and the uncertainties associated with the interpolation onto the cartesian grid. Thus, using the mean, median, 75th percentile, and 90th percentile heights appears to be a more reliable use of WSR-88D data as the resulting errors and biases are well within the expected radar sampling spacing.

Figure 6 also shows that BBD (which is much larger and heavier than other intermediate particles) is settling or sinking much faster as opposed to the smoke particles that are likely to remain suspended for much longer, which could create differences in the injection heights recorded for downwind regions and contribute to the uncertainty. Another minor note is that the WSR-88D records data approximately every 6–7 min for extended periods of time, but the airborne lidar records data continuously for shorter periods of time–therefore, the time comparison is not exact, further adding some uncertainty to this comparison.

Overall, usage of these retrievals is only recommended in the vicinity of the fire, for which the overall, average percentage difference was small (Table 2). Further, to capture the maximum injection heights of a fire with WSR-88D retrievals over the whole grid, an appropriate percentile (of the WSR-88D-derived heights) would need to be determined. Mean and bias metrics were computed, presented in Table 1, using the lidar-derived maximum heights and the 75th-90th percentiles of WSR-88D-derived heights, resulting in ~600 m mean error and bias

KRISHNA ET AL. 8 of 13

21698996, 2024, 9, Downloaded from https://agupubs.onlinelibrary.wiley.com/doi/10.1029/2023JD039926 by University Of California, Los, Wiley Online Library on [03/07/2024]. See the Terms and Conditions (https://onlinelibrary.wiley.com/emm/emm/emm.)

-conditions) on Wiley Online Library for rules of use; OA articles are governed by the applicable Creat

Detailed Description of Injection Heights Derived From Both WSR-88D (R) and Airborne Lidar (L) Data in Meters

Date (PST)	Time (PST)	R_{max} (m)	L_{max} (m)	R_{mean} (m)	L_{mean} (m)	R_{median} (m)	L_{median} (m)	R_{75th_p} (m)	L_{75th_p} (m)	R_{90th_p} (m)	L_{90th_p} (m)
3 Aug 2019	14:00	5,410	3,310	3,590	3,020	3,860	3,010	4,380	3,220	5,410	3,310
	15:00	6,450	4,450	3,480	3,000	3,340	3,000	4,380	3,160	5,410	3,280
	17:00	5,930	4,450	3,800	3,220	3,860	3,100	4,380	3,420	4,890	4,000
	18:00	6,450	4,420	3,280	3,470	3,340	3,430	3,860	3,620	4,380	4,270
	19:00	5,410	3,940	3,710	3,230	3,860	3,070	4,380	3,550	4,890	3,910
6 Aug 2019	14:00	5,410	3,970	3,270	3,280	3,340	3,250	3,860	3,470	4,380	3,700
7 Aug 2019	16:00	9,040	7,090	5,210	5,230	5,410	5,130	6,450	5,770	6,970	6,890
	18:00	9,560	7,420	5,420	5,250	5,410	5,500	5,930	5,930	6,970	6,970
	19:00	9,040	6,340	4,630	5,330	4,380	5,320	5,410	5,530	6,450	6,040
Mean bias [m]		1,920		151		221		596		820	
Mean % bias		40.0%		5.7%		8.5%		17.1%		22.7%	
Mean error [m]		1,920		356		470		622		820	
Mean % error		40.0%		10.0%		13.3%		17.5%		22.7%	

Note. Listed are the distributions of hourly maximum (R_{max}, L_{max}) , mean (R_{mean}, L_{mean}) , and median (R_{median}, L_{median}) injection heights. The heights in the following table correspond to the maximum heights retrieved at the time the aircraft was airborne. Lidar-derived heights are retrieved according to the flight path and WSR-88D-derived heights are retrieved within the pre-determined grid. All values are rounded to 3 significant figures.

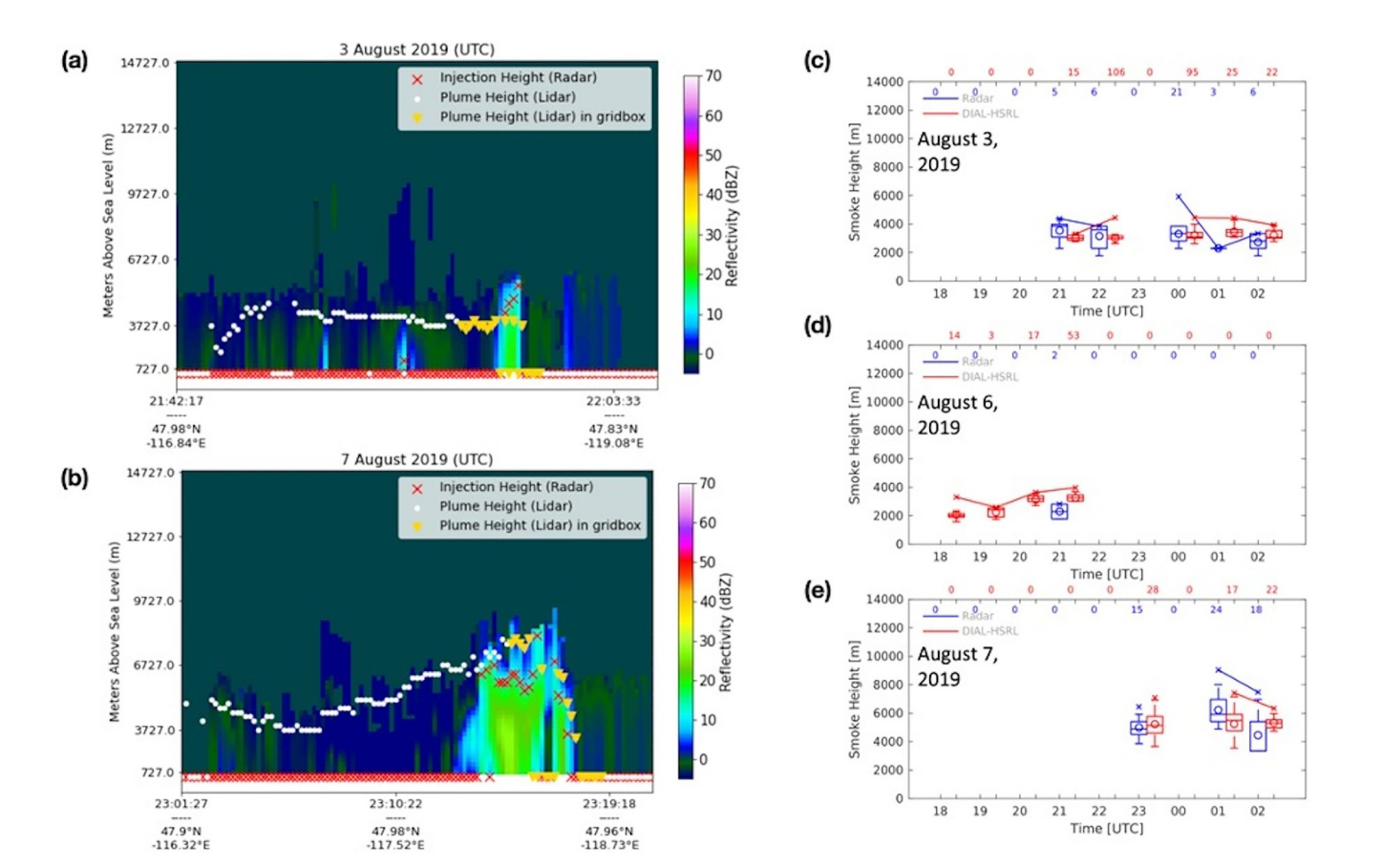


Figure 6. Left panels: Temporal cross-sections of reflectivity according to sections of the flight paths on (a) 3 August 2019 and (b) 7 August 2019. Injection heights are super-imposed on the cross-section. WSR-88D derived injection heights are highlighted in red for both plots. Lidar-derived injection heights within the pre-determined grid are highlighted as yellow triangles. All other lidar-derived heights are shown as white dots. **Right panels:** Similar to Figure 5, but using WSR-88D data mapped according to the flight track for (a) 3 August 2019, (b) 6 August 2019, and (c) 7 August 2019.

KRISHNA ET AL. 9 of 13

Table 2Further Details on Figure 6

Date (PST)	Time (PST)	R_{max} (m)	L_{max} (m)	R_{mean} (m)	L_{mean} (m)	R _{median} (m)	L_{median} (m)	R_{75th_p} (m)	L_{75th_p} (m)	R_{90th_p} (m)	L_{90th_p} (m)
3 Aug 2019	14:00	4,380	3,310	3,550	3,020	3,860	3,010	3,990	3,220	4,380	3,310
	15:00	3,860	4,450	3,170	3,000	3,600	3,000	3,860	3,160	3,860	3,280
	17:00	5,930	4,450	3,310	3,220	3,340	3,100	3,860	3,420	4,060	4,000
	18:00	2300	4,420	2,300	3,470	2,300	3,430	2,300	3,620	2,300	4,270
	19:00	3,340	3,940	2,730	3,230	2,820	3,070	3,340	3,550	3,340	3,910
6 Aug 2019	14:00	2,820	3,970	2,300	3,280	2,300	3,250	2,820	3,470	2,820	3,700
7 Aug 2019	16:00	6,450	7,090	5,000	5,230	4,890	5,130	5,410	5,770	5,930	6,890
	18:00	9,040	7,420	6,230	5,250	5,930	5,500	6,970	5,930	8,110	6,970
	19:00	7,490	6,340	4,460	5,330	3,340	5,320	5,410	5,530	6,810	6,040
Mean bias [m]		24.4		-220		-270		32.2		-84.4	
Mean % bias		-1.0%		-6.1%		-5.4%		0.8%		-2.0%	
Mean error [m]		1,160		613		741		623		889	
Mean % error		24.4%		16.1%		19.6%		16.2%		19.9%	

Note. Similar to Table 1, but with WSR-88D data mapped according to the flight track for the appropriate days.

ranging from -2% to 13%. Hence, WSR-88D-derived heights within the 75th-90th percentile range would appropriately capture the maximum injection heights, given the >1 km expected radar beam spacing at these heights.

Distinct to the 2019 Williams Flats Fire event were the occurrences of fire-generated thunderstorms (pyrocumulonimbus or 'pyroCbs' for short) around 06 UTC on 8 August 2019 and 00 UTC on 9 August 2019 (Peterson et al., 2022). The DC-8 aircraft flew on 8 August 2019 and sampled the latter pyroCbs. Lidar retrievals for these flights were not included in the analysis given that the aircraft sampled smoke and anvils mostly downwind of the pre-determined grid, primarily due to safety issues. However, the WSR-88D-derived heights can be compared to the anvil heights derived in Ye et al. (2021), which are between 9 and 10 km during 00–03 UTC on 9 August 2019. Shown in Figure 3, the maximum heights for this temporal range are \sim 13 km, showing a similar overprediction as the other days. Despite this, the heights in the 75th-90th percentiles are within the 5–8 km range, below the maximum injection heights. Thus, a larger percentile may need to be used to better capture the top injection heights for pyroCbs.

4. Conclusions

We have shown that it is possible to fully resolve the diurnal and day-to-day behavior of wildfires using WSR-88D dual polarization data to estimate the injection heights of smoke plumes using BBD as a surrogate for smoke aerosol particles in the vicinity of the fire. The injection height estimation algorithm, which was constructed with the help of previous observations of polarimetric data characteristic to smoke plumes (i.e., Reflectivity $Z \ge 10$ dBZ and correlation coefficient 0.2 < C.C. < 0.9), was able to estimate the injection heights of BBD at regular time intervals for most of the life-span of a fire, except when fire activity was low, resulting in no radar signals. The extended time series of injection heights derived from the WSR-88D data depicted a strong diurnal variability of injection heights, with the deepest smoke injections during the latter half of the day.

To validate the injection height estimation algorithm, the derived injection heights were compared to injection height retrievals from airborne lidar data. For a given time, data from a single WSR-88D was used to retrieve the maximum injection heights within the pre-determined grid whereas the lidar data were retrieved along the flight path. Results indicate that statistical metrics such as the mean, median, 75th percentile, and 90th percentile heights were well captured (350–820 m mean error). However, the maximum injection heights were consistently over predicted (40% on average) likely due to outliers resulting from the coarsening of the radar vertical beam spacing with higher altitudes. Reflectivity profiles were plotted over time according to the flight path of the aircraft; these location-specific injection height retrievals within the vicinity of the fire yielded better results for maximum injection heights but similar errors for other metrics. Results show that the true maximum smoke injection heights

KRISHNA ET AL. 10 of 13

generally correspond to the radar heights between the 75th and 90th percentile, except for the pyroCbs for which a larger percentile value may be needed.

While WSR-88D data allows for the retrieval of real-time smoke injection measurements and for the analyses of the diurnal behavior of smoke plumes, several sources of uncertainty persist. Location-specific comparisons of injection heights derived from both WSR-88D and lidar data seem to indicate that as the distance from the source of the fire increases, the accuracy of the injection heights (estimated from the WSR-88D data) decreases. Future work to develop a more advanced algorithm may also involve accounting for how debris particles are likely to behave when suspended in the atmosphere using numerical models. Another source of uncertainty would be whether the reflectivity and correlation coefficient thresholds are optimal for the accurate estimation of injection heights. Currently, these values have been chosen using prior observations of polarimetric data, however since reflectivity and correlation coefficient values vary from fire to fire, other classifiers may need to be explored. Additionally, other WSR-88D returns that happen at low altitude such as ground clutter and anomalous propagation (that don't play a role for the fire analyzed here) would also need to be filtered out for other fires. This could be done using additional radar observables (e.g., spectrum width, radial velocity) and machine learning algorithms (Saide et al., 2023). Lastly, rapid changes in fire characteristics may correspond to rapid changes in buoyant updraft, thus making the Doppler velocity a key consideration for future, more advanced algorithms (Kingsmill et al., 2023; Rodriguez et al., 2020). Future work will need to compare the capability of estimating injections from WSR-88D data with other methods of estimating injection heights, such as those involving satellites that use passive remote sensing.

While having inherent uncertainties, the near full-time coverage of WSR-88D-derived smoke injection heights from operational weather surveillance radars has the potential to help monitor the conditions of fires in a real-time manner. It can also be used in a variety of applications including the evaluation of smoke injection approaches in the context of air quality and atmospheric composition modeling (Thapa et al., 2022; Ye et al., 2021), supporting the identification of pyroconvection (Peterson et al., 2022), and assessing historical trends of smoke injection (Wilmot et al., 2022). Future work involving multiple fires could be facilitated using data from the Multi-Radar/ Multi-Sensor (MRMS) System, which combines information from multiple radars at a spatial resolution of 1 km (Zhang et al., 2005, 2011).

Conflict of Interest

The authors declare no conflicts of interest relevant to this study.

Data Availability Statement

NOAA Next Generation Radar (NEXRAD) Level II data that can be accessed in the NOAA National Centers for Environmental Information repository (NOAA National Weather Service (NWS) Radar Operations Center, 1991), was used in the algorithm described in this manuscript. Also used within the algorithm to process and interpret the WSR-88D data, is the Python ARM Radar Toolkit, Py-ART version 1.11.6 (Helmus & Collis, 2016). The FIREX-AQ data, used to evaluate the results of the algorithm described in the manuscript, is archived by the National Aeronautics and Space Administration, U.S. Government (NASA/LARC/SD/ASDC, 2020). GOES-17 satellite imagery (used in some figures) is also available in the FIREX-AQ repository. The code for the algorithm, figures, tables, and data analysis are written in Python (Python version 3.9.7), available under the license https://www.python.org and MATLAB version R2020b (The MathWorks Inc, 2020), available at https://www.mathworks.com. The Python code is written with the help of several libraries, including NumPy version 1.21.2 (Harris et al., 2020) under the license https://numpy.org, Matplotlib version 3.4.3 (Hunter, 2007) under the license https://www.matplotlib. org, SciPy version 1.2.1 (Virtanen et al., 2020) under the license https://scipy.org, and Pandas version 1.2.5 (McKinney, 2010; The pandas development team, 2021) under the license https://pandas.pydata.org. Some figures were also made with the help of Microsoft PowerPoint version 16.75 (Microsoft Corporation, 2023), Keynote version 13.1 (Apple Inc, 2023); Adobe Illustrator 2023 version 27.4.1 (Adobe Inc, 2023). Code associated with this manuscript is published on GitHub (https://github.com/mansakrishna23/Injection_ Height Estimation Algorithm) and Zenodo (https://doi.org/10.5281/zenodo.8306303).

KRISHNA ET AL. 11 of 13



Journal of Geophysical Research: Atmospheres

10.1029/2023JD039926

Acknowledgments

This work has been supported by the following grants: NSF 2013461, NSF 2238338, NASA 80NSSC18K0629, NOAA NA18OAR4310107.

References

Adobe Inc. (2023). Adobe Illustrator 2023 (version 27.4.1). Retrieved from https://www.adobe.com/products/illustrator

Amiridis, V., Giannakaki, E., Balis, D. S., Gerasopoulos, E., Pytharoulis, I., Zanis, P., et al. (2010). Smoke injection heights from agricultural burning in Eastern Europe as seen by CALIPSO. Atmospheric Chemistry and Physics, 10(23), 11567–11576. https://doi.org/10.5194/acp-10-11567-2010

Apple Inc. (2023). Keynote (version 13.1). Retrieved from https://www.apple.com/keynote

Balmes, J. R. (2020). The changing nature of wildfires: Impacts on the health of the public. Clinics in Chest Medicine, 41(4), 771–776. https://doi.org/10.1016/j.ccm.2020.08.006

Banta, R. M., Olivier, L. D., Holloway, E. T., Kropfli, R. A., Bartram, B. W., Cupp, R. E., & Post, M. J. (1992). Smoke-column observations from two forest fires using Doppler lidar and Doppler radar. *Journal of Applied Meteorology and Climatology*, 31(11), 1328–1349. https://doi.org/ 10.1175/1520-0450(1992)031<1328:SCOFTF>2.0.CO;2

Buchholz, R. R., Park, M., Worden, H. M., Tang, W., Edwards, D. P., Gaubert, B., et al. (2022). New seasonal pattern of pollution emerges from changing North American wildfires. *Nature Communications*, 13(1), 2043. https://doi.org/10.1038/s41467-022-29623-8

Burgess, D., & Ray, P. S. (1986). Principles of radar. In Mesoscale meteorology and forecasting (pp. 85-117).

Carr, J. L., Wu, D. L., Daniels, J., Friberg, M. D., Bresky, W., & Madani, H. (2020). GEO–GEO stereo-tracking of atmospheric motion vectors (AMVs) from the geostationary ring. *Remote Sensing*, 12(22), 3779. https://doi.org/10.3390/rs12223779

Chen, X., Wang, J., Xu, X., Zhou, M., Zhang, H., Castro Garcia, L., et al. (2021). First retrieval of absorbing aerosol height over dark target using TROPOMI oxygen B band: Algorithm development and application for surface particulate matter estimates. *Remote Sensing of Environment*, 265, 112674. https://doi.org/10.1016/j.rse.2021.112674

Crum, T. D., & Alberty, R. L. (1993). The WSR-88D and the WSR-88D operational support facility. Bulletin of the American Meteorological Society, 74(9), 1669–1688. https://doi.org/10.1175/1520-0477(1993)074<1669:TWATWO>2.0.CO;2

Crum, T. D., Saffle, R. E., & Wilson, J. W. (1998). An update on the NEXRAD program and future WSR-88D support to Operations. Weather and Forecasting, 13(2), 253–262. https://doi.org/10.1175/1520-0434(1998)013<0253; AUOTNP>2.0.CO;2

Deb, P., Moradkhani, H., Abbaszadeh, P., Kiem, A. S., Engstrom, J., Keellings, D., & Sharma, A. (2020). Causes of the widespread 2019-2020 Australian Bushfire season. *Earth's Future*, 8(11). https://doi.org/10.1029/2020EF001671

Doviak, R. J., Bringi, V., Ryzhkov, A., Zahrai, A., & Zrnić, D. (2000). Considerations for polarimetric upgrades to operational WSR-88D radars. Journal of Atmospheric and Oceanic Technology, 17(3), 257–278. https://doi.org/10.1175/1520-0426(2000)017<0257:CFPUTO>2.0.CO;2

Gakidou, E., Afshin, A., Abajobir, A. A., Abate, K. H., Abbafati, C., Abbas, K. M., et al. (2017). Global, regional, and national comparative risk assessment of 84 behavioural, environmental and occupational, and metabolic risks or clusters of risks, 1990–2016: A systematic analysis for the global burden of disease study 2016. *The Lancet*, 390(10100), 1345–1422. https://doi.org/10.1016/S0140-6736(17)32366-8

Hair, J., Hostetler, C., Cook, A., Harper, D., Notari, A., Fenn, M., et al. (2018). New capability for ozone dial profiling measurements in the troposphere and lower stratosphere from aircraft. EPJ Web of Conferences, 176, 01006. https://doi.org/10.1051/epjconf/201817601006

Harris, C. R., Millman, K. J., van der Walt, S. J., Gommers, R., Virtanen, P., Cournapeau, D., et al. (2020). Array programming with NumPy. Nature, 585(7825), 357–362. https://doi.org/10.1038/s41586-020-2649-2

Hasler, A. F. (1981). Stereographic observations from geosynchronous satellites: An important new tool for the atmospheric sciences. *Bulletin of the American Meteorological Society*, 62(2), 194–212. https://doi.org/10.1175/1520-0477(1981)062<0194:SOFGSA>2.0.CO;2

Helmus, J., & Collis, S. (2016). The Python ARM radar Toolkit (Py-ART), a library for working with weather radar data in the Python programming language. *Journal of Open Research Software*, 4(1), e25. https://doi.org/10.5334/jors.119

Higuera, P. E., & Abatzoglou, J. T. (2021). Record-setting climate enabled the extraordinary 2020 fire season in the western United States. *Global Change Biology*, 27(1), 1–2. https://doi.org/10.1111/gcb.15388

Holleman, I., Huuskonen, A., & Taylor, B. (2022). Solar monitoring of the NEXRAD WSR-88D network using operational scan data. *Journal of Atmospheric and Oceanic Technology*, 39(2), 193–205. https://doi.org/10.1175/JTECH-D-20-0204.1

Hsu, N. C., Lee, J., Sayer, A. M., Kim, W., Bettenhausen, C., & Tsay, S.-C. (2019). VIIRS deep blue aerosol products over land: Extending the EOS long-term aerosol data records. *Journal of Geophysical Research: Atmospheres*, 124(7), 4026–4053. https://doi.org/10.1029/201815020688

Hung, W.-T., Lu, C.-H., Shrestha, B., Lin, H.-C., Lin, C.-A., Grogan, D., et al. (2020). The impacts of transported wildfire smoke aerosols on surface air quality in New York state: A case study in summer 2018. Atmospheric Environment, 227, 117415. https://doi.org/10.1016/j.atmosenv.2020.117415

Hunter, J. D. (2007). Matplotlib: A 2D graphics environment. Computing in Science and Engineering, 9(3), 90–95. https://doi.org/10.1109/ MCSE.2007.55

Jones, T. A., & Christopher, S. A. (2009). Injection heights of biomass burning debris estimated from WSR-88D radar observations. IEEE Transactions on Geoscience and Remote Sensing, 47(8), 2599–2605. https://doi.org/10.1109/TGRS.2009.2014225

Kingfield, D. M., & French, M. M. (2022). The influence of WSR-88D intra-volume scanning strategies on thunderstorm observations and warnings in the dual-polarization radar Era: 2011–20. Weather and Forecasting, 37(2), 283–301. https://doi.org/10.1175/WAF-D-21-0127.1

Kingsmill, D. E., French, J. R., & Lareau, N. P. (2023). In situ microphysics observations of intense pyroconvection from a large wildfire. Atmospheric Chemistry and Physics, 23(1), 1–21. https://doi.org/10.5194/acp-23-1-2023

Lang, T. J., Rutledge, S. A., Dolan, B., Krehbiel, P., Rison, W., & Lindsey, D. T. (2014). Lightning in wildfire smoke plumes observed in Colorado during summer 2012. Monthly Weather Review, 142(2), 489–507. https://doi.org/10.1175/MWR-D-13-00184.1

Lee, J., Hsu, N. C., Bettenhausen, C., Sayer, A. M., Seftor, C. J., & Jeong, M.-J. (2015). Retrieving the height of smoke and dust aerosols by synergistic use of VIIRS, OMPS, and CALIOP observations. *Journal of Geophysical Research: Atmospheres*, 120(16), 8372–8388. https://doi.org/10.1002/2015JD023567

Liu, H., & Chandrasekar, V. (2000). Classification of hydrometeors based on polarimetric radar measurements: Development of fuzzy logic and neuro-fuzzy systems, and in situ verification. *Journal of Atmospheric and Oceanic Technology*, 17(2), 140–164. https://doi.org/10.1175/1520-0426(2000)017<0140:COHBOP>2.0.CO;2

Loría-Salazar, S. M., Sayer, A. M., Barnes, J., Huang, J., Flynn, C., Lareau, N., et al. (2021). Evaluation of novel NASA moderate resolution imaging spectroradiometer and visible infrared imaging radiometer suite aerosol products and assessment of smoke height boundary layer ratio during extreme smoke events in the western USA. *Journal of Geophysical Research: Atmospheres*, 126(11). https://doi.org/10.1029/2020JD034180

Manisalidis, I., Stavropoulou, E., Stavropoulos, A., & Bezirtzoglou, E. (2020). Environmental and health impacts of air pollution: A review. Frontiers in Public Health, 8, 14. https://doi.org/10.3389/fpubh.2020.00014

KRISHNA ET AL. 12 of 13

- McCarthy, N., Guyot, A., Dowdy, A., & McGowan, H. (2019). Wildfire and weather radar: A review. Journal of Geophysical Research: Atmospheres, 124(1), 266–286. https://doi.org/10.1029/2018JD029285
- McKinney, W. (2010). (Vol. 445, pp. 56–61). Data structures for statistical computing in Python, *Presented at the Python in Science Conference*. https://doi.org/10.25080/Majora-92bf1922-00a
- Melnikov, V. M., Zrnic, D. S., Rabin, R. M., & Zhang, P. (2008). Radar polarimetric signatures of fire plumes in Oklahoma. Geophysical Research Letters, 35(14). https://doi.org/10.1029/2008GL034311
- Michailidis, K., Koukouli, M.-E., Balis, D., Veefkind, P., de Graaf, M., Mona, L., et al. (2022). Validation of the TROPOMI/S5P aerosol layer height using EARLINET lidars. Atmospheric Chemistry and Physics Discussions, 1–30. https://doi.org/10.5194/acp-2022-412
- Microsoft Corporation. (2023). Microsoft PowerPoint (version 16.75). Retrieved from https://office.microsoft.com/PowerPoint
- NASA/LARC/SD/ASDC. (2020). FIREX-AQ DC-8 in-situ aerosol data [Dataset]. NASA Langley Atmospheric Science Data Center DAAC. https://doi.org/10.5067/ASDC/FIREXAQ_Aerosol_AircraftInSitu_DC8_Data_1
- National Research Council. (2002). Weather radar technology beyond NEXRAD. The National Academies Press. https://doi.org/10.17226/10394
 NOAA National Weather Service, National Weather Service, and US Department of Commerce. (2023). JetStream max: Volume coverage
 Patterns (VCPs). Retrieved from https://www.weather.gov/jetstream/vcp_max
- NOAA National Weather Service (NWS) Radar Operations Center. (1991). NOAA next generation radar (NEXRAD) level 2 base data [Dataset]. https://doi.org/10.7289/V5W9574V
- Peterson, D. A., Thapa, L. H., Saide, P. E., Soja, A. J., Gargulinski, E. M., Hyer, E. J., et al. (2022). Measurements from inside a thunderstorm driven by wildfire: The 2019 FIREX-AQ field experiment. *Bulletin of the American Meteorological Society*, 103(9), E2140–E2167. https://doi.org/10.1175/BAMS-D-21-0049.1
- Rodriguez, B., Lareau, N. P., Kingsmill, D. E., & Clements, C. B. (2020). Extreme pyroconvective updrafts during a megafire. *Geophysical Research Letters*, 47(18), e2020GL089001. https://doi.org/10.1029/2020GL089001
- Saide, P. E., Krishna, M., Ye, X., Thapa, L. H., Turney, F., Howes, C., & Schmidt, C. C. (2023). Estimating fire radiative power using weather radar products for wildfires. Geophysical Research Letters, 50(21), e2023GL104824. https://doi.org/10.1029/2023GL104824
- Sayer, A. M., Hsu, N. C., Lee, J., Kim, W. V., & Dutcher, S. T. (2019). Validation, stability, and consistency of MODIS collection 6.1 and VIIRS version 1 deep blue aerosol data over land. *Journal of Geophysical Research: Atmospheres*, 124(8), 4658–4688. https://doi.org/10.1029/2018JD029598
- Schum, S. K., Zhang, B., Džepina, K., Fialho, P., Mazzoleni, C., & Mazzoleni, L. R. (2018). Molecular and physical characteristics of aerosol at a remote free troposphere site: Implications for atmospheric aging. Atmospheric Chemistry and Physics, 18(19), 14017–14036. https://doi.org/10.5194/acp-18-14017-2018
- Shamsaei, K., Juliano, T. W., Roberts, M., Ebrahimian, H., Lareau, N. P., Rowell, E., & Kosovic, B. (2023). The role of fuel characteristics and heat release formulations in coupled fire-atmosphere simulation. Fire, 6(7), 264. https://doi.org/10.3390/fire6070264
- Thapa, L. H., Ye, X., Hair, J. W., Fenn, M. A., Shingler, T., Kondragunta, S., et al. (2022). Heat flux assumptions contribute to overestimation of wildfire smoke injection into the free troposphere. *Communications Earth & Environment*, 3(1), 1–11. https://doi.org/10.1038/s43247-022-00563-x
- The MathWorks Inc. (2020). MATLAB version: 9.9 (R2020b). Natick, Massachusetts, United States. Retrieved from https://www.mathworks.com
- The pandas development team. (2021). pandas-dev/pandas: Pandas 1.2.5 (Version 1.2.5). https://doi.org/10.5281/zenodo.5013202
- Thurston, W., Kepert, J. D., Tory, K. J., Fawcett, R. J. B., Thurston, W., Kepert, J. D., et al. (2017). The contribution of turbulent plume dynamics to long-range spotting. *International Journal of Wildland Fire*, 26(4), 317–330. https://doi.org/10.1071/WF16142
- Tory, K. J., Thurston, W., & Kepert, J. D. (2018). Thermodynamics of pyrocumulus: A conceptual study. *Monthly Weather Review*, 146(8), 2579–2598. https://doi.org/10.1175/MWR-D-17-0377.1
- Val Martin, M., Kahn, R. A., & Tosca, M. G. (2018). A global analysis of wildfire smoke injection heights derived from space-based multi-angle imaging. Remote Sensing, 10(10), 1609. https://doi.org/10.3390/rs10101609
- Val Martin, M., Logan, J. A., Kahn, R. A., Leung, F.-Y., Nelson, D. L., & Diner, D. J. (2010). Smoke injection heights from fires in north America: Analysis of 5 years of satellite observations. Atmospheric Chemistry and Physics, 10(4), 1491–1510. https://doi.org/10.5194/acp-10-1491-2010
- Veefkind, J. P., Aben, I., McMullan, K., Förster, H., de Vries, J., Otter, G., et al. (2012). TROPOMI on the ESA sentinel-5 precursor: A GMES mission for global observations of the atmospheric composition for climate, air quality and ozone layer applications. Remote Sensing of Environment, 120, 70–83. https://doi.org/10.1016/j.rse.2011.09.027
- Virtanen, P., Gommers, R., Oliphant, T. E., Haberland, M., Reddy, T., Cournapeau, D., et al. (2020). SciPy 1.0: Fundamental algorithms for scientific computing in Python. *Nature Methods*, 17(3), 261–272. https://doi.org/10.1038/s41592-019-0686-2
- Warneke, C., Schwarz, J. P., Dibb, J., Kalashnikova, O., Frost, G., Al-Saad, J., et al. (2023). Fire influence on regional to global Environments and air quality (FIREX-AQ). *Journal of Geophysical Research: Atmospheres*, 128(2), e2022JD037758. https://doi.org/10.1029/2022JD037758
- Wilmot, T. Y., Mallia, D. V., Hallar, A. G., & Lin, J. C. (2022). Wildfire plumes in the Western US are reaching greater heights and injecting more aerosols aloft as wildfire activity intensifies. *Scientific Reports*, 12(1), 12400. https://doi.org/10.1038/s41598-022-16607-3
- Winker, D. M., Hunt, W. H., & Hostetler, C. A. (2004). Status and performance of the CALIOP lidar. Laser Radar Techniques for Atmospheric Sensing, 5575, 8–15. https://doi.org/10.1117/12.571955
- Ye, X., Arab, P., Ahmadov, R., James, E., Grell, G. A., Pierce, B., et al. (2021). Evaluation and intercomparison of wildfire smoke forecasts from multiple modeling systems for the 2019 Williams Flats fire. *Atmospheric Chemistry and Physics*, 21(18), 14427–14469. https://doi.org/10.5194/acp-21-14427-2021
- Ye, X., Saide, P. E., Hair, J., Fenn, M., Shingler, T., Soja, A., et al. (2022). Assessing vertical allocation of wildfire smoke emissions using observational constraints from airborne lidar in the western U.S. *Journal of Geophysical Research: Atmospheres*, 127(21), e2022JD036808. https://doi.org/10.1029/2022JD036808
- Zhang, J., Howard, K., & Gourley, J. J. (2005). Constructing three-dimensional multiple-radar reflectivity mosaics: Examples of convective storms and stratiform rain echoes. *Journal of Atmospheric and Oceanic Technology*, 22(1), 30–42. https://doi.org/10.1175/JTECH-1689.1
- Zhang, J., Howard, K., Langston, C., Vasiloff, S., Kaney, B., Arthur, A., et al. (2011). National mosaic and multi-sensor QPE (NMQ) system: Description, results, and future plans. *Bulletin of the American Meteorological Society*, 92(10), 1321–1338. https://doi.org/10.1175/2011bams-d-11-00047.1
- Zrnic, D., Zhang, P., Melnikov, V., & Mirkovic, D. (2020). Of fire and smoke plumes, polarimetric radar characteristics. *Atmosphere*, 11(4), 363. https://doi.org/10.3390/atmos11040363

KRISHNA ET AL. 13 of 13